Master's Thesis

Dual additives (lithium nitrate, Lithium difluoro(bisoxalato)phosphate) to improve the electrochemical performance of Ni-rich cathode coupled with Ultra-thin lithium metal anode

Young Joon Ahn

Department of Energy Engineering

(Battery Science and Technology)

Graduate School of UNIST

2020

Dual additives (lithium nitrate, Lithium difluoro(bisoxalato)phosphate) to improve the electrochemical performance of Ni-rich cathode coupled with Ultra-thin lithium metal anode

Young Joon Ahn

Department of Energy Engineering

(Battery Science and Technology)

Graduate School of UNIST

Dual additives (lithium nitrate, Lithium difluoro(bisoxalato)phosphate)
to improve the electrochemical performance of Ni-rich cathode coupled with Ultra-thin lithium metal anode

A thesis/dissertation
submitted to the Graduate School of UNIST
in partial fulfillment of the
requirements for the degree of
Master of Science

Young Joon Ahn

6/12/2020
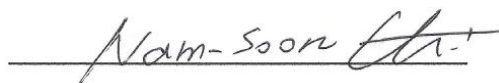
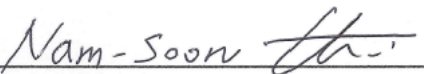Approved by
_____
Advisor
Nam-Soon Choi

Dual additives (lithium nitrate, Lithium difluoro(bisoxalato)phosphate) to improve the electrochemical performance of Ni-rich cathode coupled with Ultra-thin lithium metal anode

Young Joon Ahn

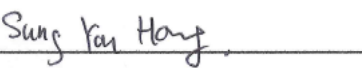This certifies that the thesis/dissertation of Young Joon Ahn is approved.
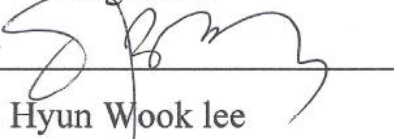
6/12/2020

signature

Nam-Soon Choi

Advisor: Nam-Soon Choi

signature

Sung You Hong

Sung You Hong

signature

Hyun Wook lee

Hyun Wook lee

Abstract

Ni-rich layered oxide cathode (Ni> 80%) and lithium metal anode are strong candidates for high energy density batteries. However, the commercialization is limited due to the morphological instability of the Ni-rich cathode, low coulombic efficiency of lithium metal, and vertical growth of dendrites. Herein, we minimize the distance between the cathode and the anode to increase limit current density and add a dual additive to form a stable solid electrolyte interphase (SEI) layer on the anode and cathode surface. Concentrated ether-based electrolytes containing lithium nitrate ($LiNO_3$) and lithium difluoro (bisoxalato) phosphate (LiDFBP) improves the capacity retention (80%) in a 20 μm $Li|LiNi_{0.8}Co_{0.1}Mn_{0.1}O_2$ full cell, with a high Coulombic efficiency of 99.5% after 245 cycles at 0.9 C rate. This paper, which improves the battery performance through optimization of cell structure (distance between electrodes) and stabilization of the interface, is expected to help in various lithium metal battery research in the future.

Contents

List of figures

Figure 17. XRD patterns of NCM811 after 40cycle. (a) Reference electrolyte (2M LiFSI DME), (b) with 1%LiDFBP, (c) with 5%LiNO$_3$, (d) with 5%LiNO$_3$, 1%LiDFBP.

Figure 18. Cross section SEM image of NCM811 after 40 cycle. (a) Reference electrolyte (2M LiFSI DME), (b) with 1%LiDFBP, (c) with 5%LiNO$_3$, (d) with 5%LiNO$_3$, 1%LiDFBP.

Figure 19. F 1s spectra of NCM811 cathode after 40 cycles. (a) Reference electrolyte (2M LiFSI DME), (b) with 1%LiDFBP, (c) with 5%LiNO$_3$, (d) with 5%LiNO$_3$, 1%LiDFBP.

Figure 20. (a) Precycle voltage profiles of Li/Cu cell with various electrolyte. Reference electrolyte was 2M LiFSI DME (DME) and distance between electrodes was 0.2mm. Capacity was 2.5 mAh cm^{-2}, and current density was 0.25 mA cm^{-2} (0.1C rate) and 40 μm lithium metal was used. (b) Visual lowest unoccupied molecular orbital (LUMO) and corresponding relative energy of each component. (c) Cu surface of Li/Cu cell after precycle. (d) In situ snapshots of the growth of lithium during the electrodeposition with an electrolyte (2M LiFSI DME+5%LiNO$_3$). (e) Li$_3$N powder purchased from Sigma-Aldrich.

Figure 21. S 2p, P 2p spectra of lithium metal anode after precycle of full cell. (a) Reference electrolyte (2M LiFSI DME), (b) with 1%LiDFBP, (c) with 5%LiNO$_3$, (d) with 5%LiNO$_3$, 1%LiDFBP.

Figure 22. SEM images of plating lithium on Cu. (a) Reference electrolyte (2M LiFSI DME), (b) with 1%LiDFBP, (c) with 5%LiNO$_3$, (d) with 5%LiNO$_3$, 1%LiDFBP. The capacity was 2.5 mAh cm^{-2} ,and current density was 0.25 mA cm^{-2}. Distance between electrodes was 0.2mm and 40 μm lithium metal was used.

Figure 23. Voltage versus time for a lithium/lithium symmetric cell with various electrolyte at 2.5 mAh cm^{-2}, 2.25 mA cm^{-2} (0.9C rate). 40 μm lithium metal was used and distance between electrodes is 0.214 mm. Reference electrolyte is 2M LiFSI DME (DME).

Figure 24. Voltage versus time for a lithium/lithium symmetric cell with various electrolyte at (a) 2 mAh cm^{-2}, 5 mA cm^{-2} (2.5 C rate) using 40 μm lithium, (b) 5 mAh cm^{-2}, 2mAcm^{-2} (0.4 C rate) using 100 μm lithium. Distance between electrodes is (a) 0.014mm, (b) 0.394 mm. Reference electrolyte is 2M LiFSI DME.

Figure 25. N 1s, P 2p spectra of lithium metal anode of full cell after 40 cycles. (a) Reference electrolyte (2M LiFSI DME), (b) with 1%LiDFBP, (c) with 5%LiNO$_3$, (d) with 5%LiNO$_3$, 1%LiDFBP.

Figure 26. (a) Cycle performance and (b) coulombic efficiency (CE) of full cells with ultra-thin 20μm lithium metal anode.

1. Introduction

1.1. Advantages of Lithium metal batteries (LMB)

As the various batteries including lithium ion batteries (LiB) have been developed[1], we were able to use camcorders, laptops, and even electric cars in recent years[2,3]. However, because LIB has reached its theoretical capacity (especially graphite anode), a new anode material is required to get a high capacity battery. (figure 1)[4,5].

Since lithium metal has the lowest electrochemical reduction potential (-3.045 V versus standard hydrogen electrode) and a high theoretical capacity (3960 mAh g^{-1}), it is receiving attention as a next-generation anode material for high energy density batteries[6–8]. Recently, research on lithium-oxygen and lithium-sulfur batteries using such lithium metal as an electrode has been increasing. [9–11]

(a)
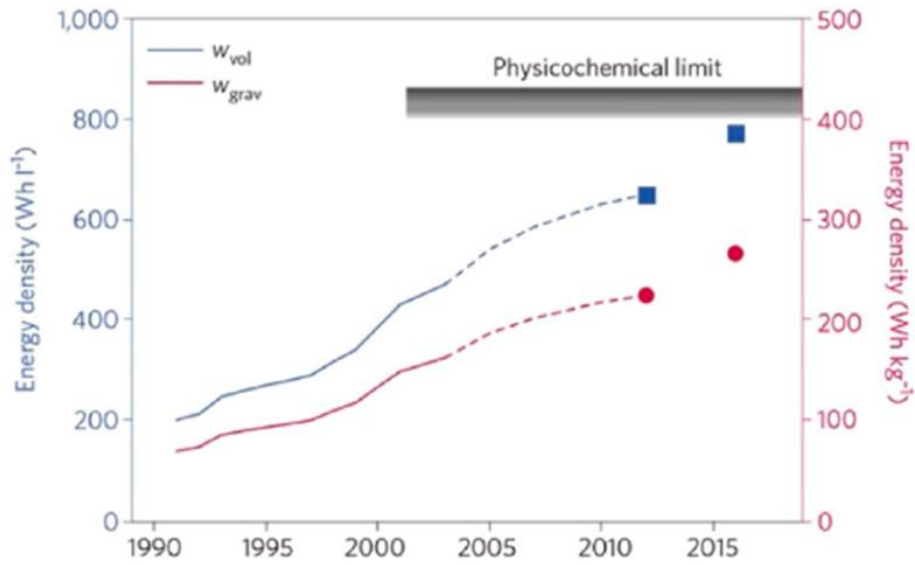
(b)
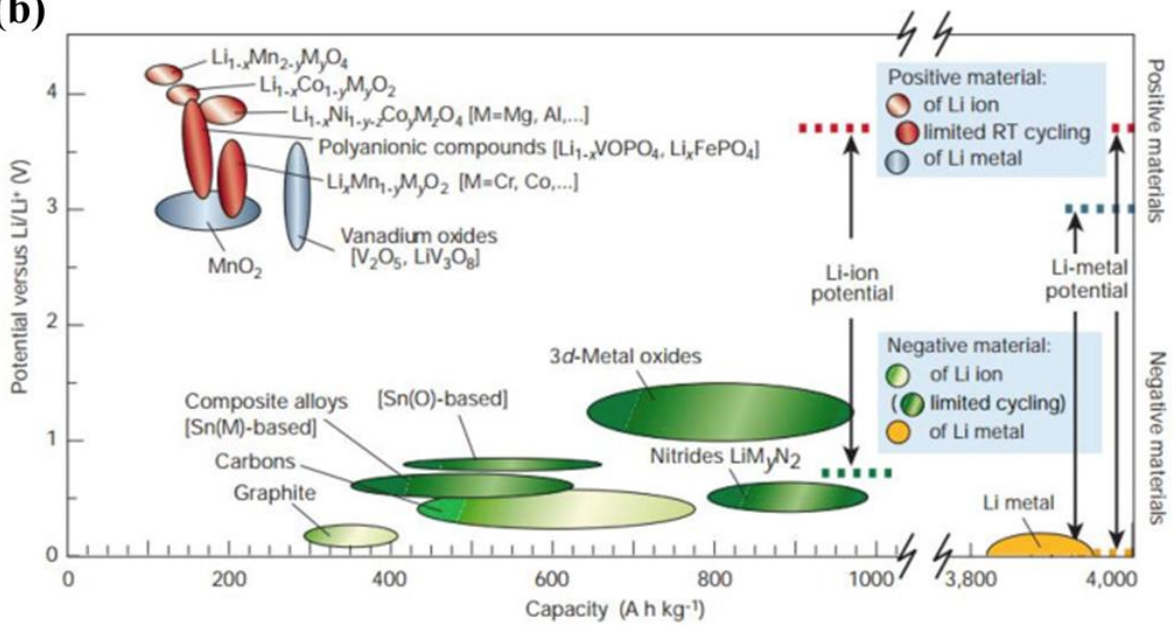
Figure 1. (a) Lithium-ion battery capacity increase status[4]. (b) Electrode material properties of secondary battery[5]

1.2. Problems of Lithium metal anode

The fact that lithium metal has a low reduction potential serves as an advantage in terms of the energy density of the battery, but it also indicates that lithium metal is a highly reactive material. Since the SEI layer is formed even when the lithium is in contact with the electrolyte, the surface area of the lithium metal anode must be reduced to reduce side reactions with the electrolyte.

Lithium, unlike graphite, is a hostless negative electrode where lithium plating occurs on the lithium metal surface. If the supply speed of lithium ions to the lithium metal surface is faster than the supply speed (current density) of electrons, lithium with large particle size in the form of a pencake[12] will be uniformly electrodeposited. Conversely, if the supply speed of electrons (current density) is faster than the supply speed of lithium ions, lithium with a small particle size will be electrodeposited unevenly, and this electrodeposition lithium is called dendrite (figure 2a).

Because the following problems occur when dendrites grow, the biggest problem in using lithium metal as an anode is lithium dendrites. (figure 2b)[6,13,14].

1) Cell short circuit

Since dendrites are very thin, when they grow, they break through the separator and touch the cathode, which is called a short circuit. If the anode and cathode are connected inside the cell by dendrites, a thermal runaway may occur and the cell may explode. It is the main reason why lithium metal anodes cannot be commercialized.

2) Further adverse reaction

Since dendrites have a larger contact area with electrolytes than dense lithium, side reactions with electrolytes increase. This causes additional consumption of the lithium, which causes low coulomb efficiency.

3) Dead lithium

When the dendrite enclosed by the SEI layer formed due to side reaction with the electrolyte falls from the current collector. In this case, all surfaces of the dendrites that are dropped are covered with an SEI layer, so they are electrochemically inert. This condition is called dead lithium and dead lithium does not participate in the reaction, so when dead lithium is formed, coulombic efficiency decreases.
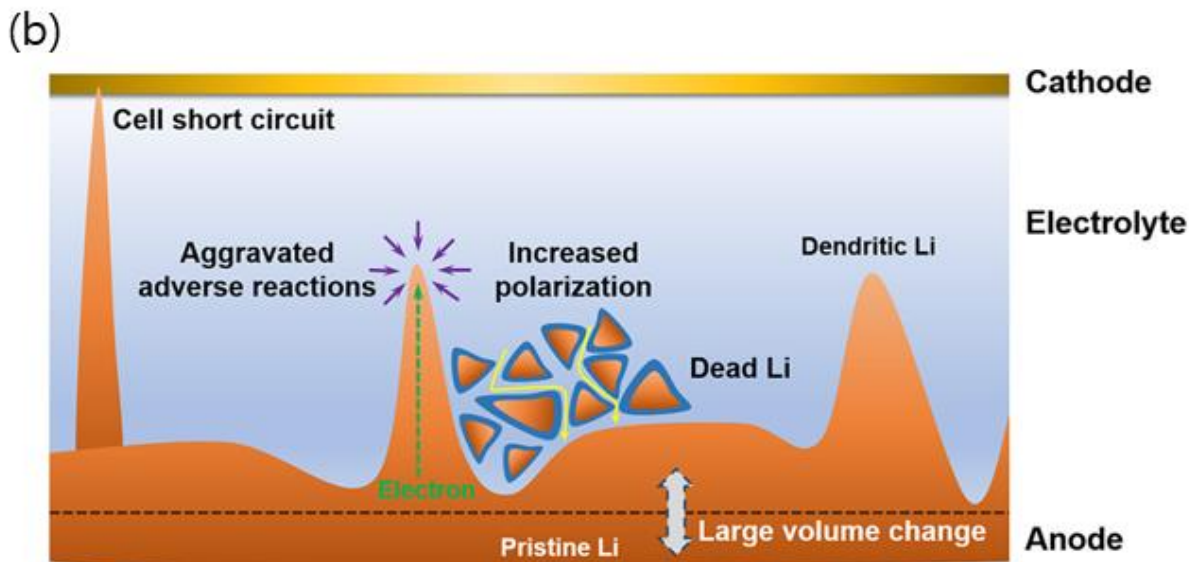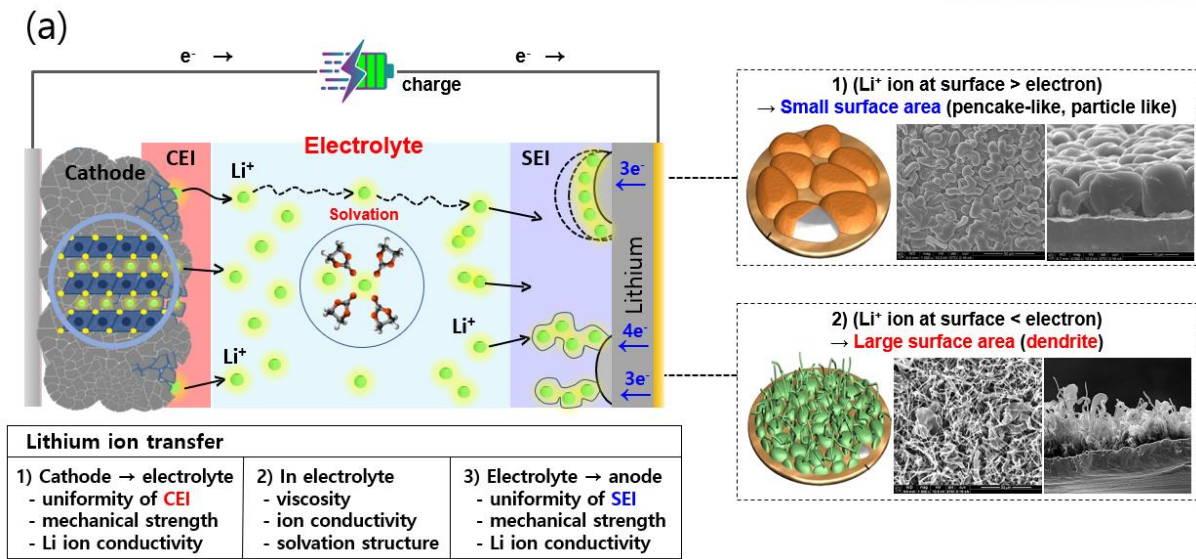
Figure 2. (a). Scheme of dendrite growth[12] (b) Various problems when forming in dendrites[6]

1.3. Strategies for improving reversibility of lithium metal anodes

1.3.1 Distance between cathode and anode

One way to increase the supply rate of lithium ions is to reduce the distance between electrodes. As the distance between the electrodes decreases, the movement distance of lithium ions becomes shorter and the supply speed increases. The concentration distribution of lithium ions at the limit current density is as follows (figure 3a). Since the supply speed of lithium ions and the supply speed of electrons coincide, the lithium ion concentration at the anode surface is zero. If the distance between electrodes becomes closer ((a) -> (b) -> (c)) at the same current density, the lithium ion concentration at the lithium interface increases, thereby suppressing the growth of dendrites (figure 3a). This represents an increase in the limiting current density and can be expressed as the following equation[15]. As the distance between electrodes gets closer (L becomes smaller), the limit current density and diffusion coefficient increase.

Limit current density
$$J = \frac{2ec\_^0D}{t\_L} \quad \text{(L : Distance between electrodes)} \tag{1}$$

Diffusion coefficient
$$D = -\frac{SL^2}{\pi^2} \quad \text{(L : Distance between electrodes)} \tag{2}$$

As a result of reversibility test of lithium metal according to the distance between electrodes, it was confirmed that the closer the distance between electrodes, the higher initial coulombic efficiency. This means a reduction in side reactions and a reduction in dead lithium (figure 3b). Also result of XPS analysis confirmed that the closer the distance between the electrodes, the thinner the film formed, which means that the consumption of the electrolyte additive can be minimized. The thinner the SEI layer, the faster the supply of lithium ions because the travel distance of the lithium ions in the SEI layer decreases (figure 3c).

However, when applying a current density lower than the limiting current density, dendrites are sometimes formed because of the influence of the SEI layer. This indicates that it is essential to form a stable SEI layer to suppress dendrites[16].
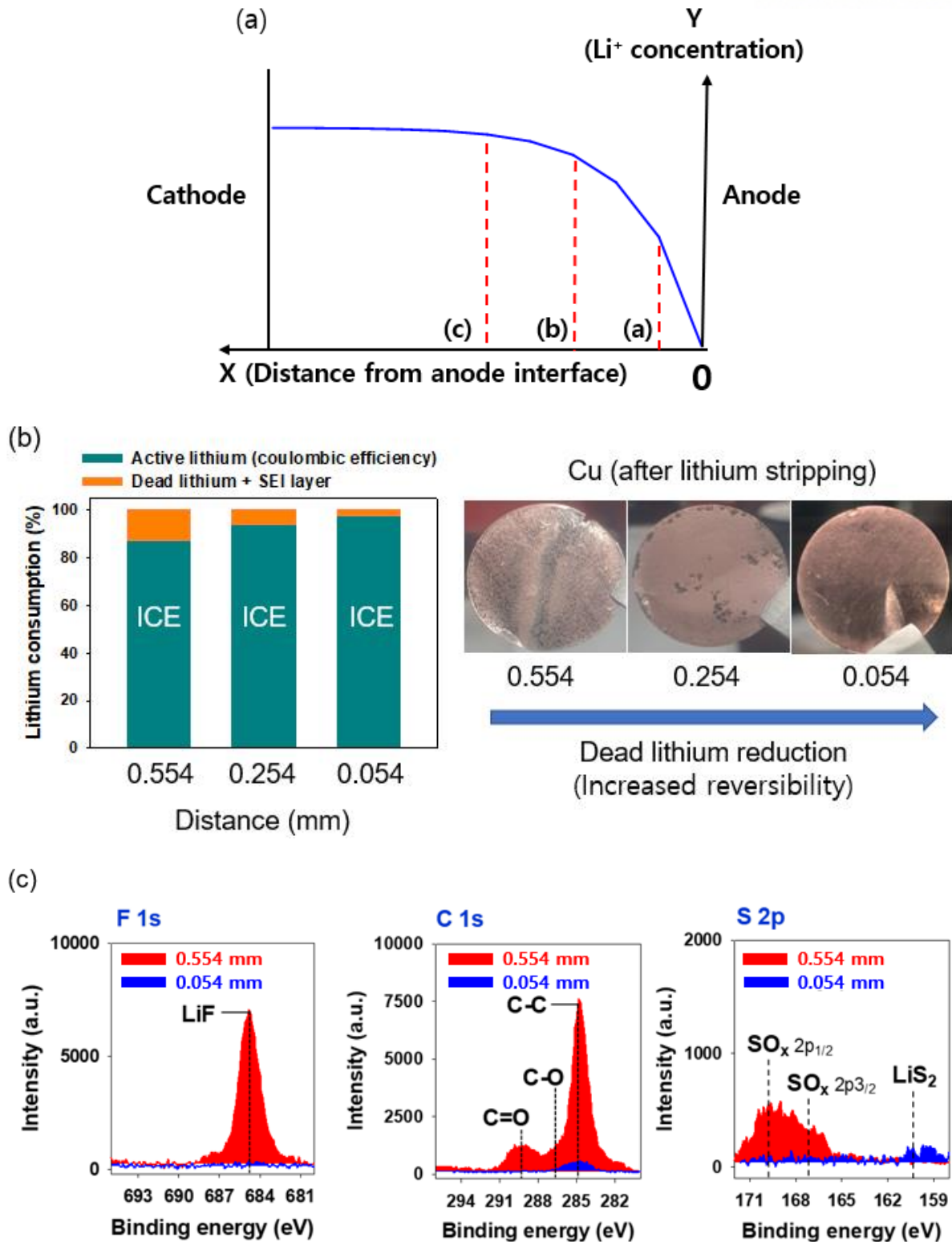
Figure 3. (a) Lithium ion concentration according to the distance from the anode surface at limit current density. (b) Initial Coulombic efficiency of Li/Cu cells according to the distance between electrodes, 2.8 mAh cm^{-2}, 0.1C for precycle, electrolyte was 2M LiFSI DME +5%LiNO$_3$+1%LiPF$_6$. (c) XPS data of plated lithium according to the distance between electrodes, electrolyte was 2M LiFSI DME.

6

1.3.2 Highly concentrated electrolytes

Many studies have been reported to form a wellstructured SEI layer on a lithium metal. When a carbonate mainly used as a solvent in LiB is used for LMB, dendritic lithium is electrodeposited and exhibits low coulombic efficiency[17,18]. To solve this, many studies have been conducted using a glmye solvent that is more stable for lithium because it has a higher LUMO energy than carbonate. However, although glyme has a small reactivity to lithium metal, it has a high HOMO energy level, resulting in an electrolyte oxidation problem[19,20].

Henderson reports that high concentration liquid electrolytes using glyme high oxidation stability[21,22]. This is because most solvents are coordination with salts when using high concentration salts.

As the concentration of the electrolyte increases, the reversibility of the lithium metal anode also improves because the composition of the film formed on the anode changes depending on the concentration of the electrolyte. At low concentrations, solvent-separated ion pairs (SSIP) exist, which means that the cations and anions of the salt are completely separated and dissociated. In this case, since there are many free-solvents, an orientation of solvents appears on the anode surface, and therefore, a solvent-derived film is formed. As the electrolyte concentration increases (> 2M), the anion participating in the solvation sheath increases, so the solvation structure changes from SSIP to contact ion pairs (CIP) and cation-anion aggregates (AGGs)[23,24]. As anions participate in the solvation structure, in a high concentration electrolyte, anions are arranged at the interface of the anode, and as a result, an anion-derived SEI layer is formed on the anode which can improve the reversibility of lithium metal[25–28] (figure 4,5).

Figure 4. (a) Formation process of SEI at low concentration electrolyte. (b) SEI formation process at highly concentrated electrolyte[27]

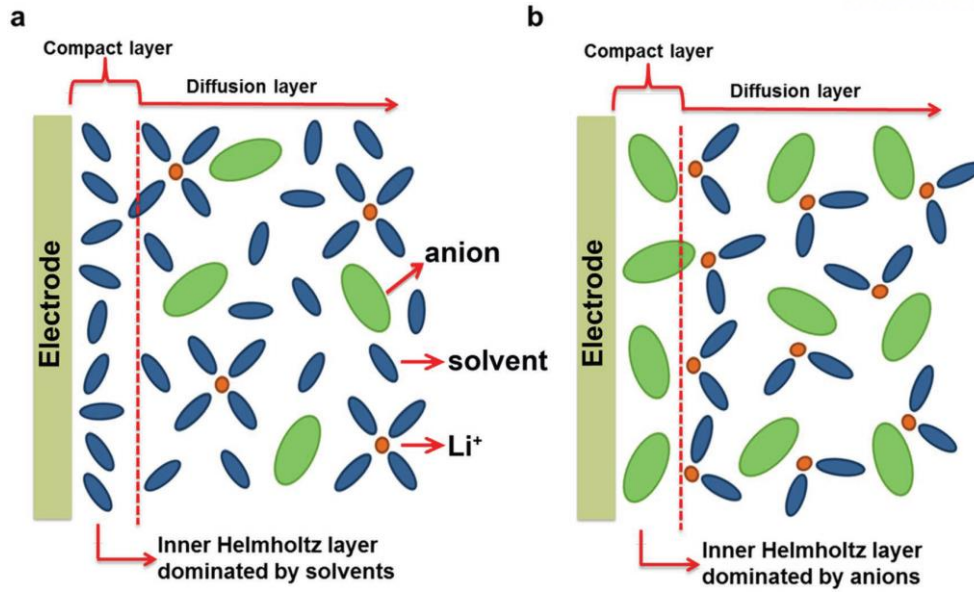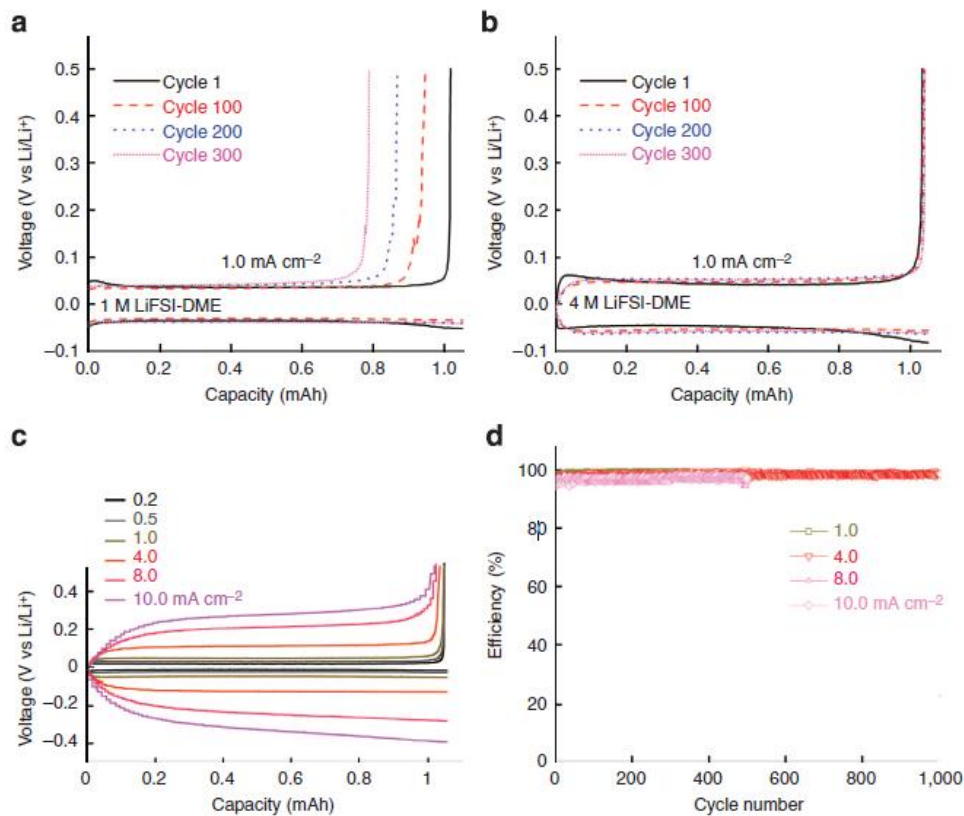**Figure 5.** (a) Voltage profiles for the Li/Cu cell with 1M LiFSI DME (b) Voltage profiles for the Li/Cu cell with 4M LiFSI DME (c) Polarization of the Li/Cu cell for the 4M LiFSI-DME electrolyte. (d) CE of Li/Cu cell with 4M LiFSI DME at different current densities[28].

1.3.3 Electrolyte additives

Various additives have been reported so far to make a wellstructured SEI layer on a lithium. (FEC[29–31], VC[32,33], LiNO$_3$[34-50]). Particularly, in the case of the NO$_3^-$ anion of LiNO$_3$, the electron-donating ability is larger than that of the existing salt anion (PF$_6^{-34}$, FSI^{-35}) (figure 6,7), so that the ion dipole interaction with lithium ions is strong, forming a stable film on the lithium metal anode (LiN$_x$O$_y$[36,37], Li$_3$N[34,38,39]). According to existing studies, LiNO$_3$ is known to be reduced at ~1.6V when ether solvent is used[39,40] (figure 8). However, the reduction of LiNO$_3$ has a problem because it occurs continuously as the cycle progresses[12,41]. Due to the low solubility of LiNO$_3$, various methods have been reported for continuous supply of LiNO$_3$[34,39,41,42]. In addition, the reversibility of lithium metal anodes improved through synergy with other additives[12]. As such, LiNO$_3$ is well known for stabilizing the lithium metal interface, and is mainly used for lithium sulfur (Li-S) batteries[12,43,44].

However, there have been few cases where LiNO$_3$ has been applied to 4V class batteries, and most of them use NCM with low nickel content (Ni <80%) or LFP as cathode[34,35,38,45]. In addition, lithium metal stabilization by LiNO$_3$ is explained as a cause of battery performance improvement, there has been no report on the cathode mechanism of LiNO$_3$ in 4V class batteries to date.

Various salt type additives that form a stable film on the cathode have also been reported, such as lithium bis(oxalato)borate (LiBOB)[46,47], lithium difluoro(oxalato)borate (LiDFOB)[48,49], Lithium Difluoro(bisoxalato) Phosphate (LiDFBP)[50,51] (figure 9). In particular, LiDFBP improves the reversibility of the negative electrode by forming a stable film on the anode (decomposed at ~1.9V, figure 10).
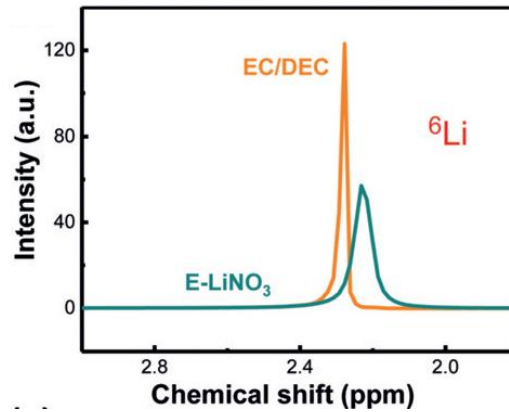
Figure 6. Nature abundance ^{6}Li NMR spectra of the electrolyte[34]. EC/DEC : 1M LiPF$_6$ EC/DEC(1/1), E-LiNO$_3$: 1M LiPF$_6$ EC/DEC(1/1)+LiNO$_3$
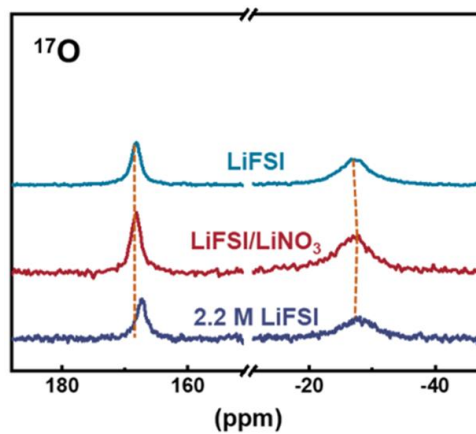
Figure 7. ^{17}O NMR spectra of various electrolytes. LiFSI : 2M LiFSI DME, LiFSI/LiNO$_3$: 2M LiFSI DME+0.2M LiNO$_3$[35]
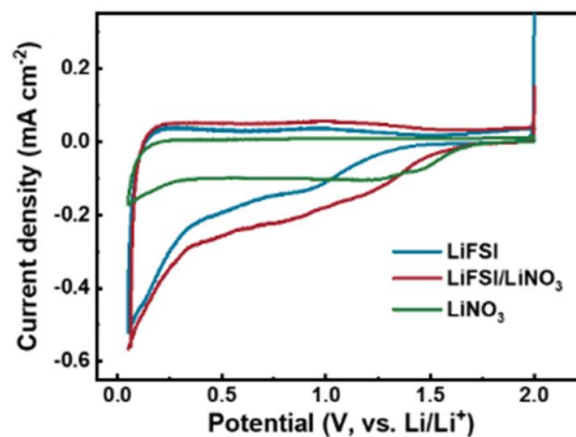
Figure 8. Cyclic voltammogram curves of various electrolyte. Working electrode is carbon-coated current collector, Li is counter and reference electrode.
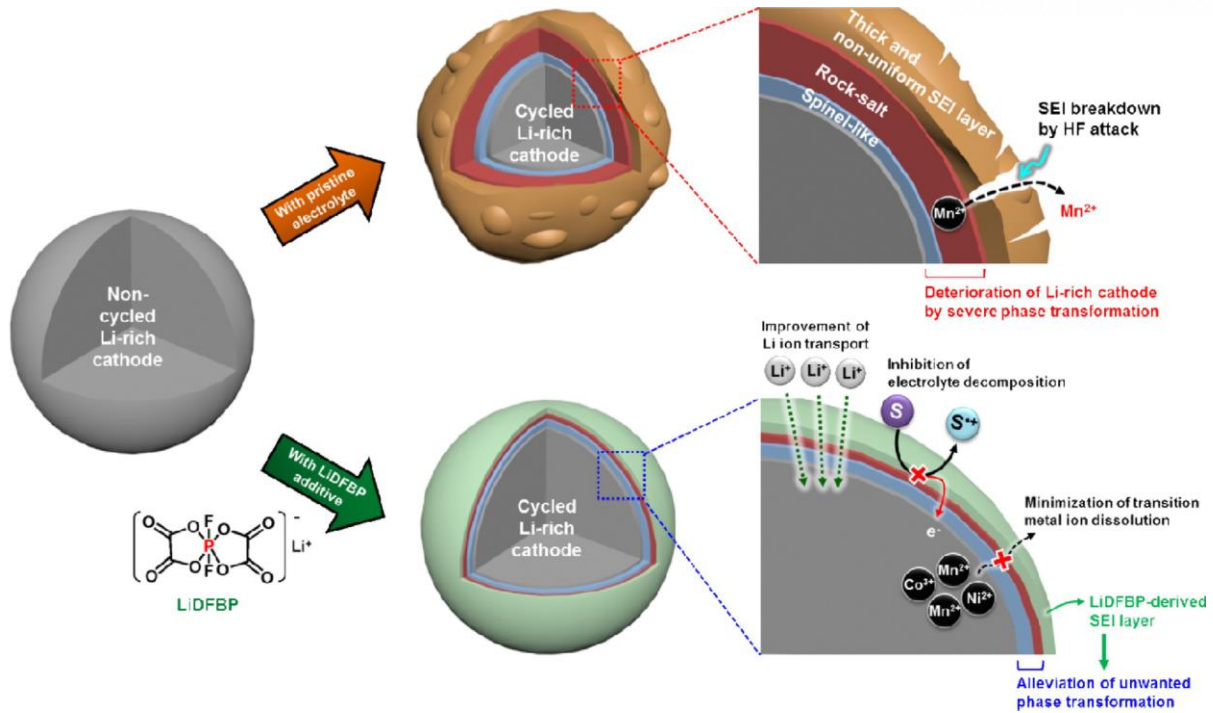
Figure 9. Schematic diagram showing the effect of LiDFBP film formation on the cathode[50].
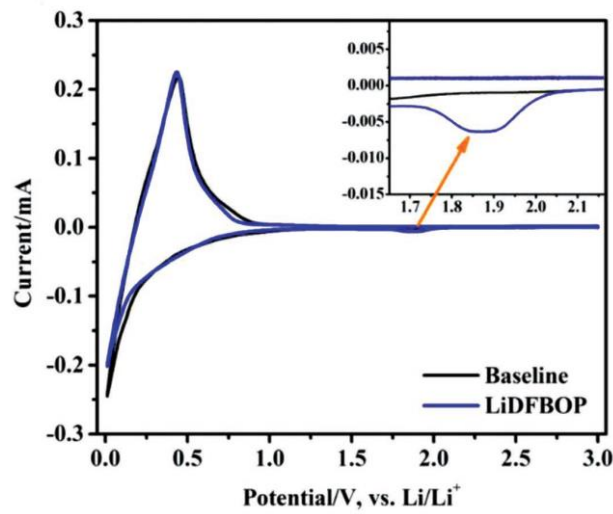
Figure 10. Cyclic voltammogram curves of electrolyte with and without LiDFBOP. Working electrode is graphite and counter electrode is lithium metal[51].

11

2. Experimental

2.1 Electrolyte and electrodes

The reference electrolyte was 2 M lithium bis(fluorosulfonyl)imide (LiFSI, ≥99.7%, Chunbo Fine Chem Co., Ltd.) dissolved in a 1,2-dimethoxyethane (DME, ≥99.9%, Sigma-Aldrich). Lithium nitrate (LiNO$_3$, ≥99.9%, Sigma-Aldrich) and lithium difluoro(bisoxalato) phosphate (LiDFBP, Chunbo Fine Chem Co., Ltd.) were added into the reference electrolyte as additives. Every electrolyte was treated by CaH$_2$ and filtered after 30 minutes.

The composite cathode electrodes were prepared by mixing 95wt.% LiNi$_{0.8}$Co$_{0.1}$Mn$_{0.1}$O$_2$ (NCM811), 2.5wt.% Super-P, and 2.5wt.% poly(vinylidene fluoride) (PVdF) dissolved in anhydrous N-methyl-2-pyrrolidinone (NMP, 99.5%, Sigma-Aldrich). The specific capacity was 3 mAh cm^{-2} and the loading of the active material was 15 mg cm^{-2}.

2.2 Electrochemical mesasurements

Coin cells were assembled in an argon-filled glove box which accommodated less than 1 ppm oxygen and moisture. The 2032 coin type full cells (NCM811 / Li) were monitored in galvanostatic mode within a voltage range of 3.0–4.2 V versus Li^+/Li using a computer-controlled battery measurement system (WonATech WBCS 3000) at 25 °C. The full cells (NCM811 / Li) were first cycled at 0.1 C. and then cycled at 0.5 C rate for three times and cycled at 0.9 C rate. To confirm the leakage current of full cells, the full cells (NCM / Li) were charged to 4.2 V at a 0.1 C rate, and then the leakage current of the cells was monitored at a constant charging voltage of 4.2 V for 10 hr. The 2032 coin type Li/Cu cells were first cycled at 0.1C. Various 2016 coin type lithium/lithium symmetric cells were evaluated under various conditions.

2.3 Characterization

Cross-sectional images of the cathodes were acquired using an ion-milling system (IM4000Plus, Hitachi) and SEM (FE-SEM; JSM-6700F, JEOL) with energy-disperse spectroscopy (XFlash 6130, Bruker). The CEI and SEI structure of the NCM811 cathodes and lithium meatal anodes were examined by ex situ X-ray photoelectron spectroscopy (XPS, Scientific K-Alpha system, Thermo Scientific). All XPS spectra were energy calibrated to the hydrocarbon peak at a binding energy of 284.8 eV. The morphology of Li deposits on a Cu substrate was observed by field-emission scanning electron microscopy (FE-SEM; JSM-6700F, JEOL) in a high-vacuum environment. The crystal structure of the NCM811 cathode was investigated by the X-ray diffraction (XRD). Bruker D2 Phaser powder diffractometer with a Cu K∂ radiation source (λ=1.54184 Å) was used. The scanning 2θ range was 10-80° at 1°/min. The electrochemical impedance spectroscopy (EIS) measurements for full cells were carried out using an IVIUM frequency response analyzer. The frequency range was from 10 mHz to 1MHz and the potentiostat signal amplitude was 5mV.

3. Result and discussion

3.1 Electrochemical performances of Li/Cathode full cells and analysis.

The cycling characteristics of the Li/NCM full cell of each electrolyte are shown in Figure 11. When each additive was used alone (figure 11a), each exhibited improved life characteristics (retention 80% reference electrolyte: 37 cycles, 1% LiDFBP: 161 cycles, 1% LiNO$_3$: 270 cycles). In the case of LiNO$_3$ (figure 11b), it can be seen that the performance is improved as the content is increased (1%LiNO$_3$: 270cycle, 3%LiNO$_3$: 325 cycle, 5%LiNO$_3$: 370 cycle), indicating that sufficient supply of LiNO$_3$ is required. However, when LiDBP and LiNO$_3$ were used together, the lifespan was slightly reduced compared to when LiNO$_3$ was used alone (5%LiNO$_3$ 370cycle, 5%LiNO$_3$+1%LiDFBP: 350 cycle based on retention 80%).

Analysis of cathode was performed to know the effect of the additives. The voltage graph for the Li/LiNi$_{0.8}$Mn$_{0.1}$Co$_{0.1}$O$_2$ full cell with four electrolyte compositions is shown in figure 12a. Although all four compositions show similar initial Coulomb efficiency, the composition of the SEI layer formed in each electrolyte composition is expected to be different because the HOMO energy levels of the salt, solvent, and additive are different (figure 12b). Since the HOMO energy level of additives (LiNO$_3$, LiDFBP) is higher than that of salt, it is expected to make a wellstructrured SEI layer on the cathode by oxidative decomposition prior to salt. As a result of the floating test (figure 12c), when the additive is applied, it can be seen that the generated current decreases, which means the additive actually forms a stable SEI layer on the cathode.

To confirm that the actual additive inhibited the decomposition of salt (LiFSI), XPS analysis of the cathode was performed after the precycle (figure 13,14). Inhibition of salt decomposition by application of additives was confirmed through reduction of LiF, SO$_x$, and Li$_2$S peaks (LiF, SO$_x$, Li$_2$S: LiFSI decomposition products). This means that the additive is preferentially decomposed to form a stable SEI layer.

The OCV measurement of the full cell after 40 cycles is as follows (figure 15a). The reference electrolyte (2M LiFSI DME) showed a reduced value compared to precycle OCV at about 1.0V. This difference was due to the increase in the resistance of the full cell (figure 15b). When applying the additive, OCV did not drop due to the small resistance. In order to find out which electrode is the main reason for the increase in resistance, the evaluation was conducted by changing the electrode of the cycle cell and the electrode of the precycle cell. In the case of the first cell (cycle NCM811 / precycle lithium), the OCV of the reference electrolyte still has a reduced value (figure 16a) than that of the precycle OCV, and the cycle evaluation did not proceed (figure 16b). For the second cell (precycle NCM811 / cycle lithium), the OCV of the reference electrolyte had a value similar to that of the precycle OCV (figure 16c), and smooth cycle evaluation was performed (figure 16d). Through this, it was confirmed that the main deterioration factor of the full cell when using the reference electrolyte was the cathode. When an additive is applied, the resistance of the full cell is reduced (figure 15b), and the activity of the cycle anode and cathode is still maintained.

Further analysis was conducted to determine what problems occurred with the cathode of the reference electrolyte and what role the additive plays to protect the cathode (figure 17,18). XRD analysis with 40 cycled NCM811 confirmed that the crystallinity of the cathode decreased when a reference electrolyte was used (figure 17a). In addition, as a result of cross-sectional SEM analysis, numerous micro-cracks of secondary particles of NCM811 were identified (figure 18a). On the other hand, when the additive was applied, it was confirmed that the crystallinity of the cathode was maintained (figure 17b,c,d) and that micro-crack did not occur in the secondary particles (figure 18b,c,d). Through this, it was confirmed

that the cathode particles are protected when the additive is applied. XPS analysis was performed with a 40 cycled NCM to determine the mechanism of the additive at the cathode (figure 19). When the additive is applied, LiF decreases (figure 19b,c,d). Considering that LiF is a decomposition product of salt (LiFSI), it can be said that the additive inhibited the decomposition of salt. That is, the additive decomposes preferentially over the salt to make a stable film on the cathode to inhibit further decomposition of the salt, which is consistent with the HOMO energy trend (figure 11b).

Through the analysis of the cathode, it was confirmed that the main deterioration factor of the reference electrolyte was the cathode, which was due to the excessive formation of LiF, a non-conductive material due to salt decomposition. When an additive with a higher HOMO energy than that of a salt is applied, the additive is preferentially decomposed to make a wellstructured film on the cathode, confirming that the cell performance is improved.
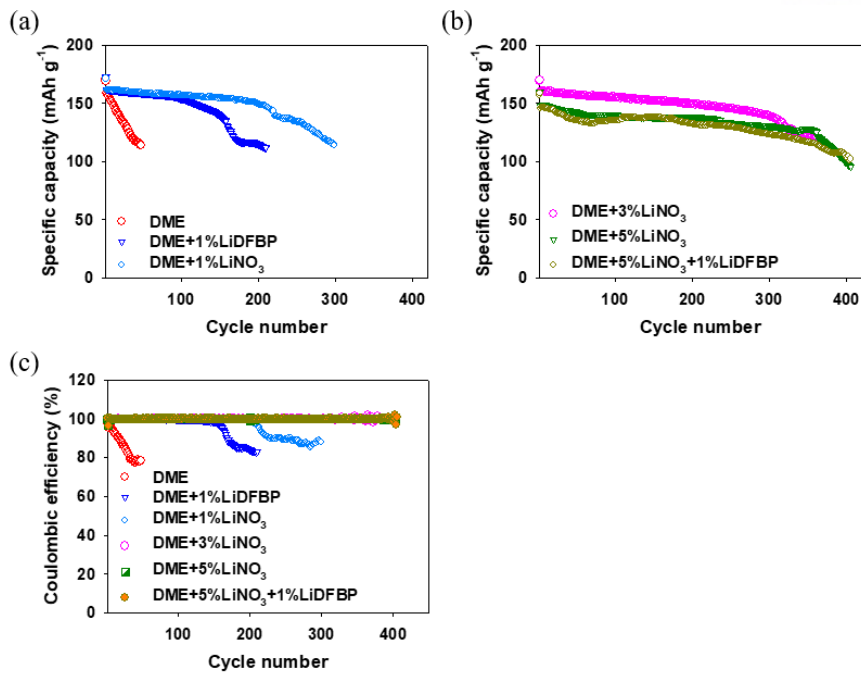
Figure 11 (a),(b) Cycling performance and (c) coulombic efficiency of (NCM811/ $40\mu m$ lithium) full cells with various electrolyte. Reference electrolyte is 2M LiFSI DME (DME).
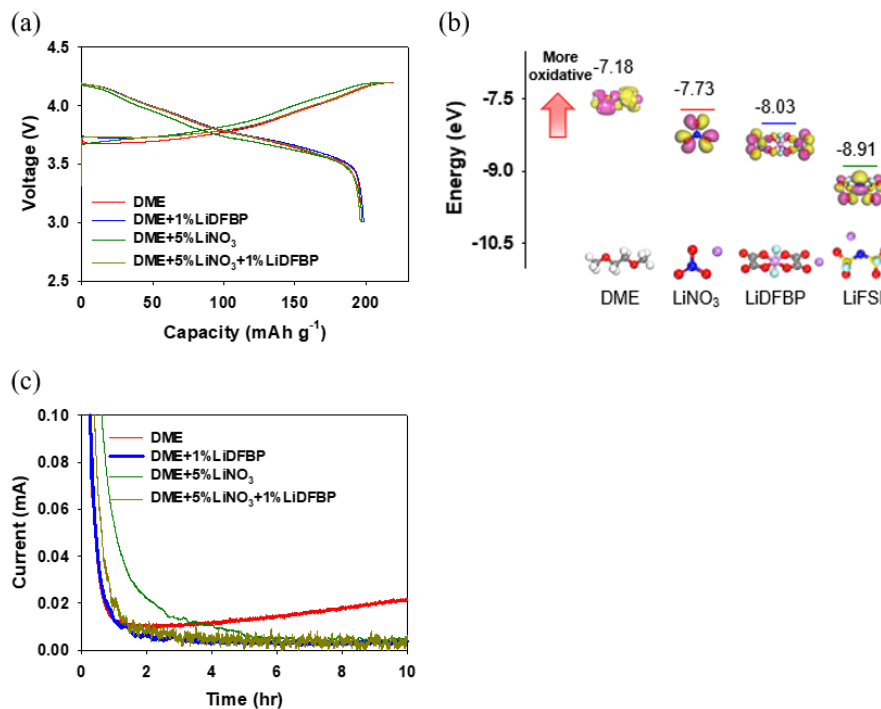
Figure 12 (a) Precycle voltage profiles of full cell with various electrolyte. (b) Visual highest occupied molecular orbital (HOMO) and corresponding relative energy of each component. (c) Electrochemical floating test of full cell at constant voltage of 4.2V after charging up to 4.2V in different electrolytes. Reference electrolyte is 2M LiFSI DME (DME).

16

Figure 13. F 1s spectra of NCM811 cathode after precycle. (a) Reference electrolyte (2M LiFSI DME), (b) with 1%LiDFBP, (c) with 5%LiNO₃, (d) with 5%LiNO₃, 1%LiDFBP.
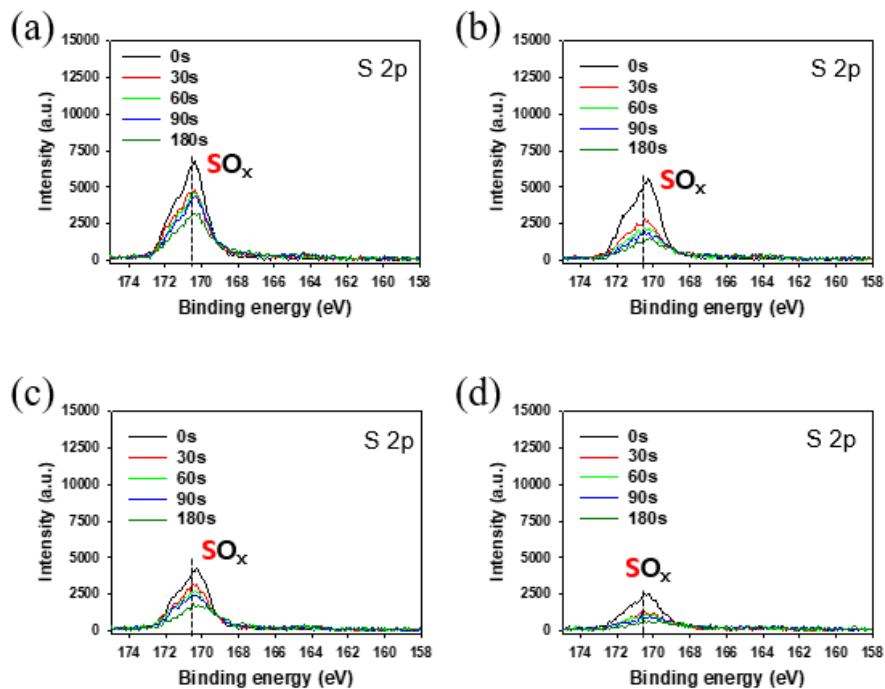
Figure 14. S 2p spectra of NCM811 cathode after precycle. (a) Reference electrolyte (2M LiFSI DME), (b) with 1%LiDFBP, (c) with 5%LiNO₃, (d) with 5%LiNO₃, 1%LiDFBP.
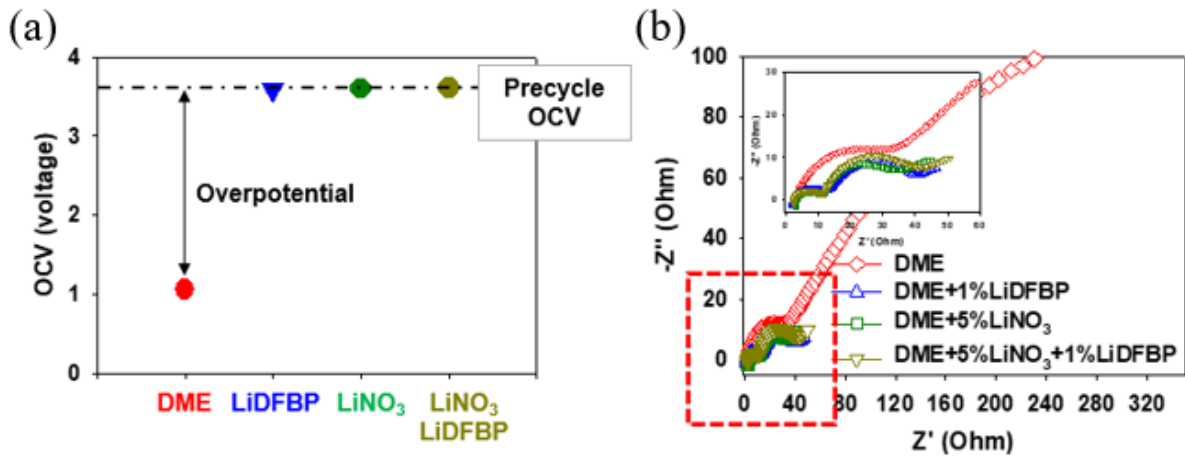
Figure 15. (a) Open circuit voltage (OCV), (b) Nyquist plots of AC impedance of NCM811/lithium metal full cell after 40 cycle for each electrolyte. Reference electrolyte is 2M LiFSI DME (DME).
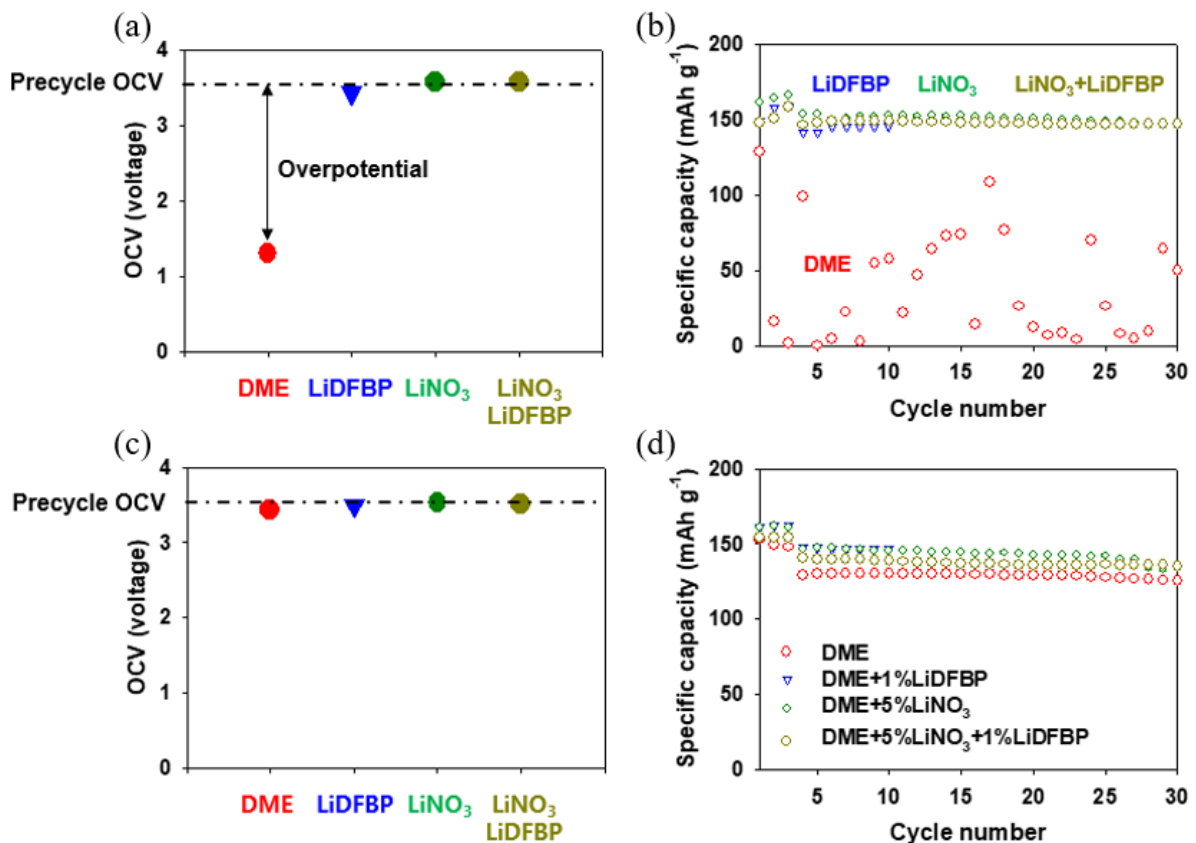
Figure 16. (a) Open circuit voltage and (b) cycling performance of full cell (40 cycled NCM811 / precycled lithium metal). (c) Open circuit voltage and (d) cycling performance of full cell (precycled NCM811 / 40 cycled lithium metal). Reference electrolyte is 2M LiFSI DME (DME).
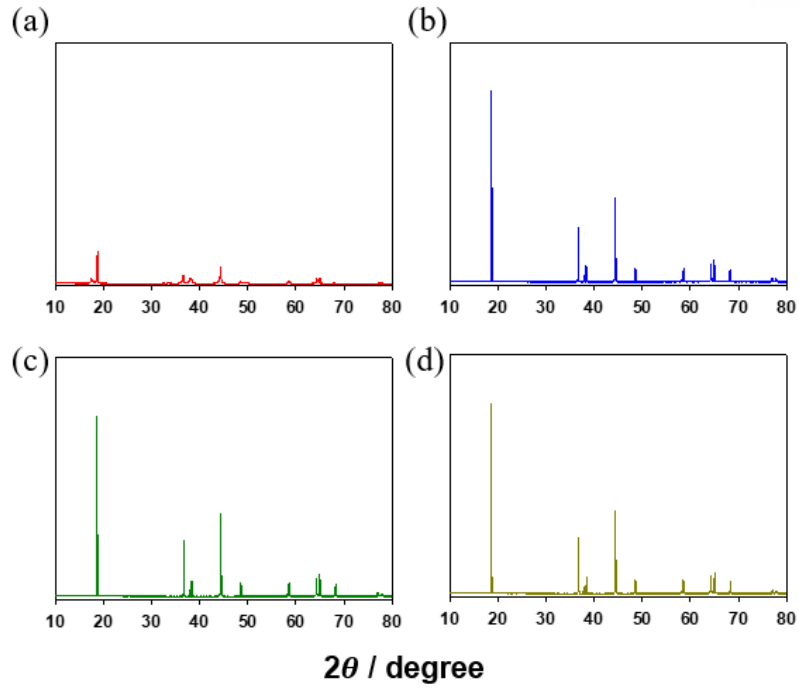
Figure 17. XRD patterns of NCM811 after 40cycle. (a) Reference electrolyte (2M LiFSI DME), (b) with 1%LiDFBP, (c) with 5%LiNO$_3$, (d) with 5%LiNO$_3$, 1%LiDFBP.
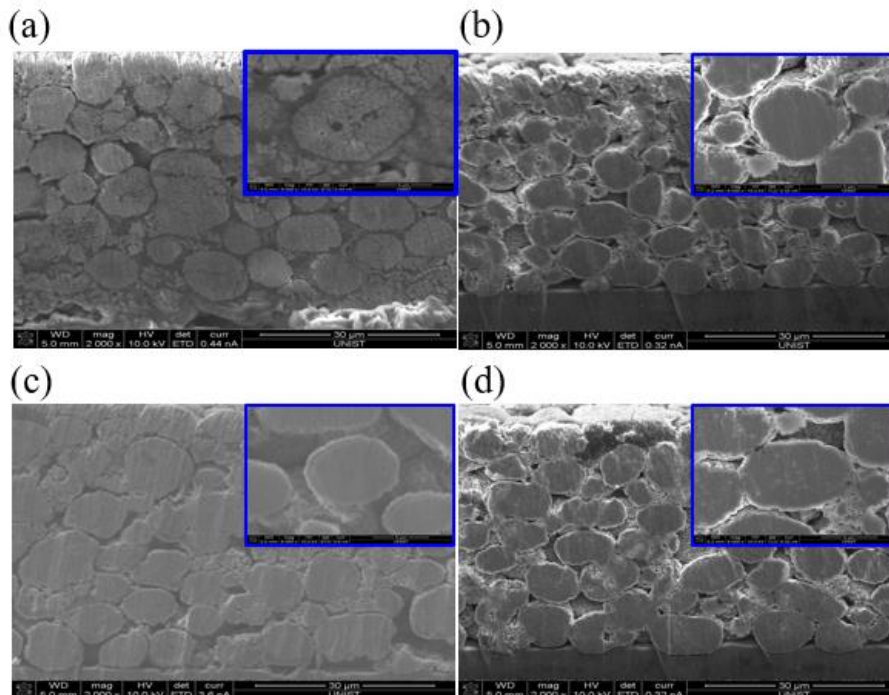
Figure 18. Cross section SEM image of NCM811 after 40 cycle. (a) Reference electrolyte (2M LiFSI DME), (b) with 1%LiDFBP, (c) with 5%LiNO$_3$, (d) with 5%LiNO$_3$, 1%LiDFBP.
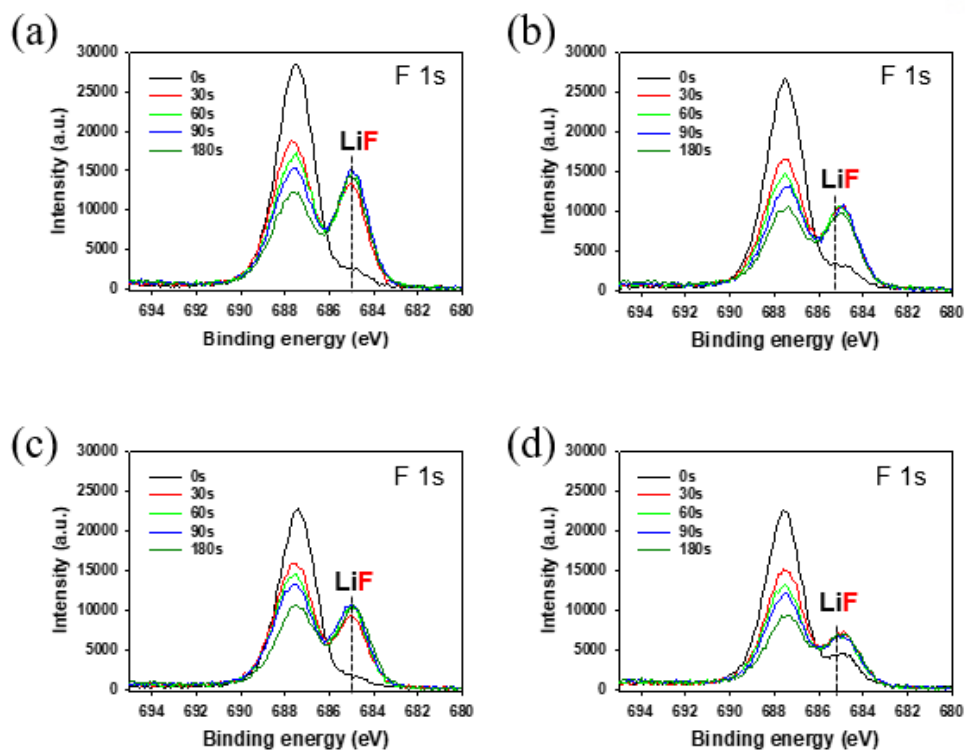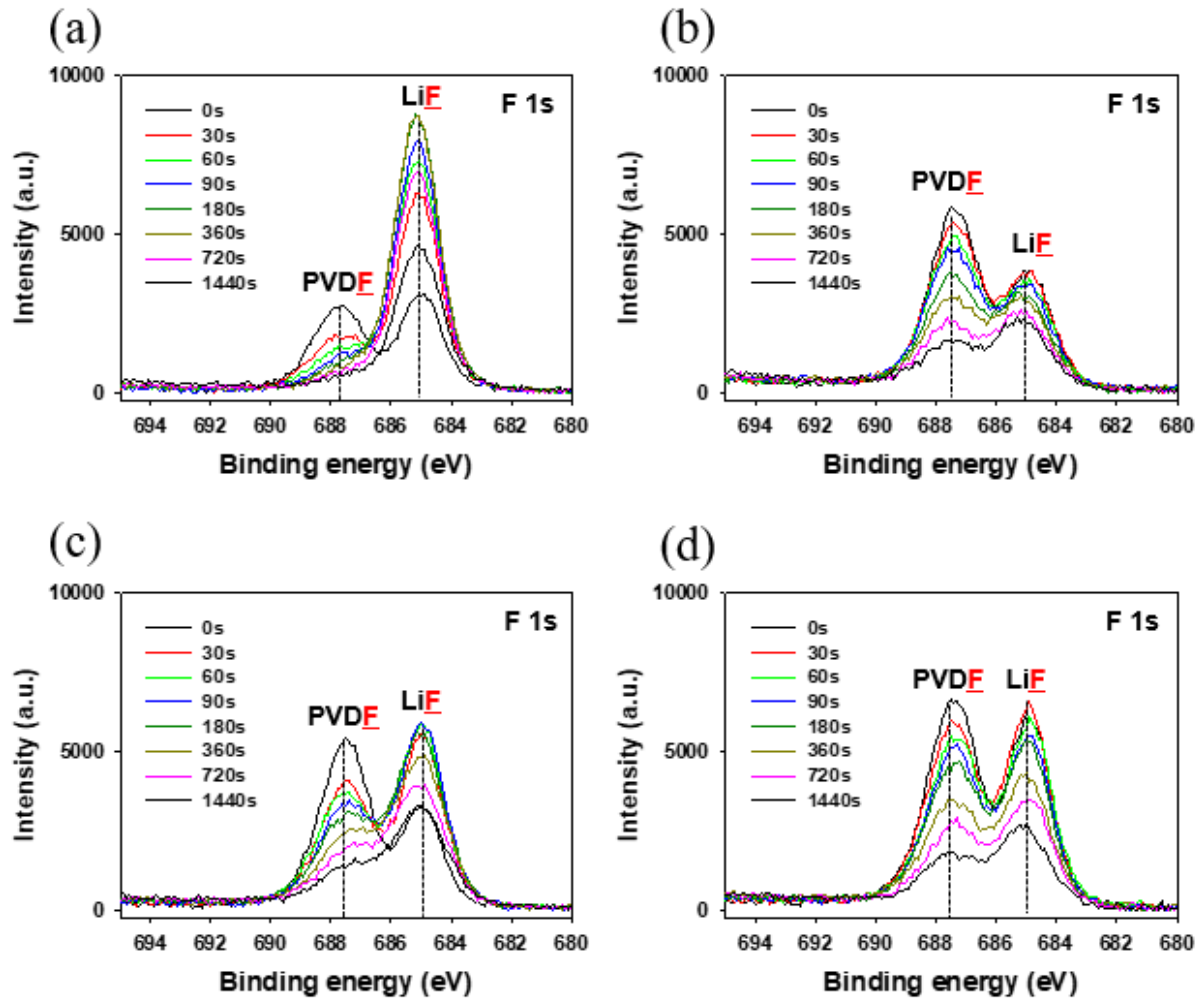
Figure 19 F 1s spectra of NCM811 cathode after 40 cycles. (a) Reference electrolyte (2M LiFSI DME), (b) with 1%LiDFBP, (c) with 5%LiNO₃, (d) with 5%LiNO₃, 1%LiDFBP.

3.2 Electrochemical performances of Li/Li, Li/Cu cells and analysis

The voltage graphs for lithium plating/stripping of the four electrolyte compositions are shown in figure 20a. Even the reference electrolyte (2M LiFSI DME) shows a high efficiency of 78.7% because the distance between the electrodes is very short (the distance between the electrodes: 0.2 mm). When an additive is applied, the reversibility of the lithium metal increases because the additive decomposes first to form a stable SEI layer. This is consistent with the LUMO energy level (figure 20b). Additives with lower LUMO enegy levels than salt (LiFSI) and solvent (DME) decompose first to make a stable SEI layer.

Especially, when $LiNO_3$ is added, it shows a high reversibility of lithium metal of more than 95%, which is consistent with the existing research that $LiNO_3$ improves the reversibility of lithium metal anodes by forming a stable film on lithium metal[34,38,39]. When observing the Cu surface after stripping (figure 20c), when using the electrolyte composition with $LiNO_3$, a black layer can be identified on the Cu surface, which is consistent with the previous research[41]. The black layer also appears when observing the lithium electrodeposition process of an electrolyte containing $LiNO_3$ using in-situ OM (figure 20d). This is presumed to be Li_3N because the Li_3N powder is black (figure 20e) which is a decomposition product of $LiNO_3$.

Inhibition of electrolyte decomposition according to the application of additives can also be confirmed through XPS analysis after precycle of the full cell (figure 21). The decrease in salt decomposition (SO_x, Li_2S) peak due to the application of the additive indicates that the decomposition of the electrolyte salt (LiFSI) can be suppressed when the additive is applied. In addition, when $LiNO_3$ and LiDFBP are used at the same time, the decomposition of LiDFBP can be minimized compared to when LiDFBP is used alone (reduction of $LiPO_xF_y$ peak, which is decomposition product of LiDFBP). Since the decomposition products of $LiNO_3$ were formed very thin, the peak intensity was very weak in the precycle cell. In the case of lithium electrodeposition morphology (figure 22), all four electrolyte compositions exhibit particle-like morphologies, because the distance between electrodes is close enough (the distance between electrodes is 0.2 mm).

However, the evaluation result of the lithium/lithium symmetric cell was different from the initial lithium reversibility evaluation (figure 23). Unlike the initial coulombic efficiency, which effectively inhibited salt decomposition and improved the reversibility of lithium metal when $LiNO_3$ was applied, in the long-term evaluation, cell performance was detoriated when $LiNO_3$ was applied (2M LiFSI DME : 236 cycle, 2M LiFSI DME+5%LiNO3 : 120 cycle). This is because $LiNO_3$ continually decomposes to form a SEI layer (overlapping of the film, depletion of additives), which is consistent with the existing reports[12,41]. There is a lot of difference from the life of the full cell (370 cycle based on retention 80%) because the reduction of lithium occurs during charging and discharging in the symmetric cell, so the reduction of $LiNO_3$ also occurs twice as much as the full cell. When LiDFBP is used with $LiNO_3$, the performance of the lithium/lithium symmetric cell increases (2M LiFSI DME+5%$LiNO_3$+1%LiDFBP : 140 cycle) because LiDFBP with low LUMO energy (figure 20b) decomposes first to suppress the continuous decomposition of $LiNO_3$. Using these phenomena, world-class lithium/lithium symmetric cell life characteristics were obtained under various evaluation conditions (figure 24). As a result of XPS (figure 25), when LiDFBP was used together with $LiNO_3$, decomposition of $LiNO_3$ could be suppressed   than when $LiNO_3$ was used alone (Li_3N peak reduction), and this was due to preferential reduction of LiDFBP. In order to maximize the effect of dual additives, 20um lithium was used to evaluate the full cell, and as a result, excellent performance was secured. (figure 26). As a result of increasing the burden on the anode side by using ultra-thin lithium, when using the dual additive, it showed very good life characteristics (2M LiFSI DME+5%$LiNO_3$+1%LiDFBP: 245 cycle based on retention 80%) .

Figure 20. (a) Precycle voltage profiles of Li/Cu cell with various electrolyte. Reference electrolyte was 2M LiFSI DME (DME) and distance between electrodes was 0.2mm. Capacity was 2.5 mAh cm^{-2}, and current density was 0.25 mA cm^{-2} (0.1C rate) and 40 μm lithium metal was used. (b) Visual lowest unoccupied molecular orbital (LUMO) and corresponding relative energy of each component. (c) Cu surface of Li/Cu cell after precycle. (d) In situ snapshots of the growth of lithium during the electrodeposition with an electrolyte (2M LiFSI DME+5%LiNO$_3$). (e) Li$_3$N powder purchased from Sigma-Aldrich.

Figure 21. S 2p, P 2p spectra of lithium metal anode after precycle of full cell. (a) Reference electrolyte (2M LiFSI DME), (b) with 1%LiDFBP, (c) with 5%LiNO$_3$, (d) with 5%LiNO$_3$, 1%LiDFBP.

22

Figure 22. SEM images of plating lithium on Cu. (a) Reference electrolyte (2M LiFSI DME), (b) with 1%LiDFBP, (c) with 5%LiNO$_3$, (d) with 5%LiNO$_3$, 1%LiDFBP. The capacity was 2.5 mAh cm^{-2} and current density was 0.25 mA cm^{-2}. Distance between electrodes was 0.2mm and 40 μm lithium metal was used.

Figure 23. Voltage versus time for a lithium/lithium symmetric cell with various electrolyte at 2.5 mAh cm^{-2}, 2.25 mA cm^{-2} (0.9C rate). 40 μm lithium metal was used and distance between electrodes is 0.214 mm. Reference electrolyte is 2M LiFSI DME (DME).

Figure 24. Voltage versus time for a lithium/lithium symmetric cell with various electrolyte at (a) 2 mAh cm^{-2}, 5 mA cm^{-2} (2.5 C rate) using 40 μm lithium, (b) 5 mAh cm^{-2}, 2mAcm^{-2} (0.4 C rate) using 100 μm lithium. Distance between electrodes is (a) 0.014mm, (b) 0.394 mm. Reference electrolyte is 2M LiFSI DME.
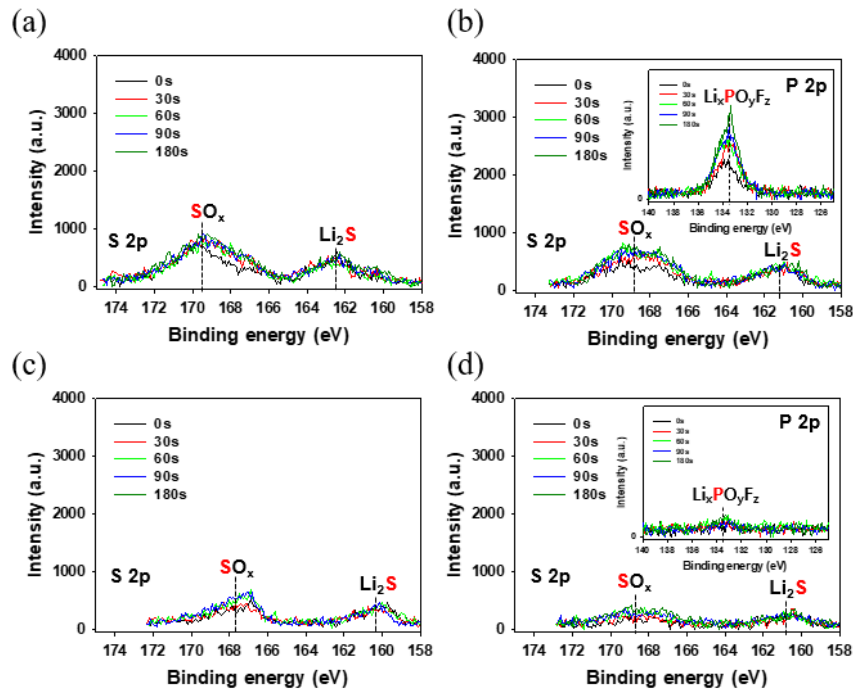

Figure 25. N 1s, P 2p spectra of lithium metal anode of full cell after 40 cycles. (a) Reference electrolyte (2M LiFSI DME), (b) with 1%LiDFBP, (c) with 5%LiNO₃, (d) with 5%LiNO₃, 1%LiDFBP.
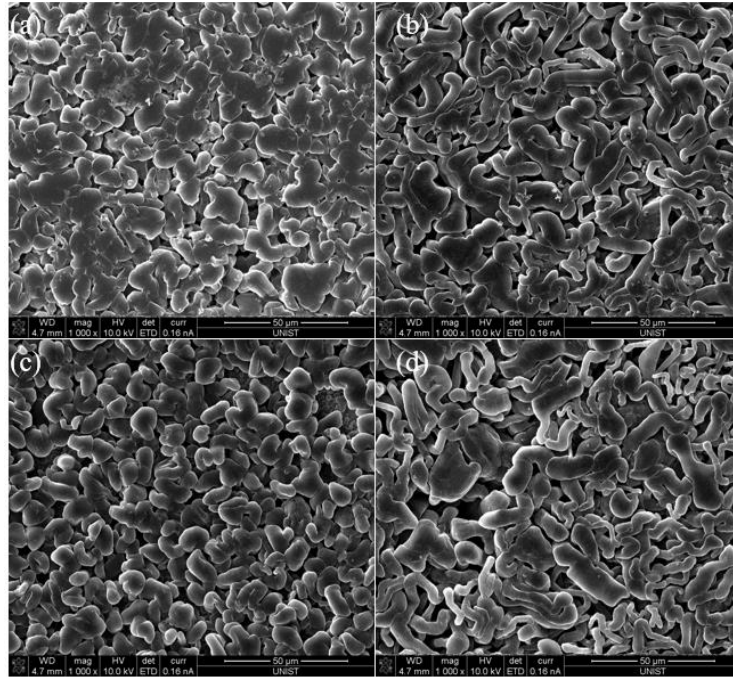
Figure 26. (a) Cycle performance and (b) coulombic efficiency (CE) of full cells with ultra-thin $20\mu m$ lithium metal anode.

4. Conclusion

Here, it is revealed that the main cause of deterioration of the reference electrolyte (2M LiFSI DME) composition full cell is due to the thick LiF film due to the continuous decomposition of the LiFSI salt. To prevent the decomposition of LiFSI at the cathode, we applied a dual additive with a HOMO energy level higher than that of LiFSI to suppress salt decomposition at the cathode. In order to solve the problem of continuous decomposition of $LiNO_3$ that occurs when using $LiNO_3$ as an additive, $LiNO_3$ is dissolved as much as possible ($5\%LiNO_3$) and the additive consumption is reduced by reducing the distance between electrodes. In addition, by using LiDFBP with a lower LUMO energy than $LiNO_3$, LiDFBP decomposes prior to $LiNO_3$ to suppress the decomposition of $LiNO_3$. Through this, we obtained world-class lithium/lithium symmetric cell lifespan results, and long life high energy density full cell (NCM811/20um lithium) lifespan results.

REFERENCES

1. Dunn, B., Kamath, H. & Tarascon, J. M. Electrical energy storage for the grid: A battery of choices. *Science* vol. 334 928–935 (2011).

2. Grande, L. *et al.* The lithium/air battery: Still an emerging system or a practical reality? *Adv. Mater.* **27**, 784–800 (2015).

3. ERIC C. EVARTS. To the limits of lithium. *Nature* **526**, S93–S95 (2015).

4. Janek, J. & Zeier, W. G. A solid future for battery development. *Nat. Energy* **1**, 1–4 (2016).

5. Liu, D. & Cao, G. Engineering nanostructured electrodes and fabrication of film electrodes for efficient lithium ion intercalation. *Energy Environ. Sci.* **3**, 1218–1237 (2010).

6. Cheng, X. B., Zhang, R., Zhao, C. Z. & Zhang, Q. Toward Safe Lithium Metal Anode in Rechargeable Batteries: A Review. *Chem. Rev.* **117**, 10403–10473 (2017).

7. Lin, D. *et al.* Three-dimensional stable lithium metal anode with nanoscale lithium islands embedded in ionically conductive solid matrix. *Proc. Natl. Acad. Sci. U. S. A.* **114**, 4613–4618 (2017).

8. Cheng, X. B. *et al.* A review of solid electrolyte interphases on lithium metal anode. *Adv. Sci.* **3**, 1–20 (2015).

9. Girishkumar, G., McCloskey, B., Luntz, A. C., Swanson, S. & Wilcke, W. Lithium-air battery: Promise and challenges. *J. Phys. Chem. Lett.* **1**, 2193–2203 (2010).

10. Ji, X., Lee, K. T. & Nazar, L. F. A highly ordered nanostructured carbon-sulphur cathode for lithium-sulphur batteries. *Nat. Mater.* **8**, 500–506 (2009).

11. Peng, H. J. *et al.* Janus separator of polypropylene-supported cellular graphene framework for sulfur cathodes with high utilization in lithium-sulfur batteries. *Adv. Sci.* **3**, 1–11 (2015).

12. Li, W. *et al.* The synergetic effect of lithium polysulfide and lithium nitrate to prevent lithium dendrite growth. *Nat. Commun.* **6**, 1–8 (2015).

13. Xu, W. *et al.* Lithium metal anodes for rechargeable batteries. *Energy Environ. Sci.* **7**, 513–537 (2014).

14. Aurbach, D. Identification of Surface Films Formed on Lithium in Propylene Carbonate Solutions. *J. Electrochem. Soc.* **134**, 1611 (1987).

15. Li, S. *et al.* Developing High-Performance Lithium Metal Anode in Liquid Electrolytes: Challenges and Progress. *Adv. Mater.* **30**, 1–29 (2018).

16. Chang, H. J. *et al.* Correlating Microstructural Lithium Metal Growth with Electrolyte Salt Depletion in Lithium Batteries Using 7 Li MRI. *J. Am. Chem. Soc.* **137**, 15209–15216 (2015).

17.   Ding, F. *et al.* Dendrite-free lithium deposition via self-healing electrostatic shield mechanism. *J. Am. Chem. Soc.* **135**, 4450–4456 (2013).

18.   Koike, S., Fujieda, T., Wakabayashi, N. & Higuchi, S. Electrochemical and quartz microbalance technique studies of anode material for secondary lithium batteries. *J. Power Sources* **68**, 480–482 (1997).

19.   Lv, D. *et al.* Failure mechanism for fast-charged lithium metal batteries with liquid electrolytes. *Adv. Energy Mater.* **5**, 1–7 (2015).

20.   Lu, Y., Tu, Z. & Archer, L. A. Stable lithium electrodeposition in liquid and nanoporous solid electrolytes. *Nat. Mater.* **13**, 961–969 (2014).

21.   Henderson, W. A. Glyme-lithium salt phase behavior. *J. Phys. Chem. B* **110**, 13177–13183 (2006).

22.   Henderson, W. A. *et al.* Glyme-lithium bis(trifluoromethanesulfonyl)imide and glyme-lithium bis(perfluoroethanesulfonyl)imide phase behavior and solvate structures. *Chem. Mater.* **17**, 2284–2289 (2005).

23.   Wan, C. *et al.* Natural abundance 17O, 6Li NMR and molecular modeling studies of the solvation structures of lithium bis(fluorosulfonyl)imide/1,2-dimethoxyethane liquid electrolytes. *J. Power Sources* **307**, 231–243 (2016).

24.   Fong, K. D. *et al.* Ion Transport and the True Transference Number in Nonaqueous Polyelectrolyte Solutions for Lithium Ion Batteries. *ACS Cent. Sci.* **5**, 1250–1260 (2019).

25.   Nie, M. *et al.* Role of solution structure in solid electrolyte interphase formation on graphite with LiPF6 in propylene carbonate. *J. Phys. Chem. C* **117**, 25381–25389 (2013).

26.   Yamada, Y. *et al.* Unusual stability of acetonitrile-based superconcentrated electrolytes for fast-charging lithium-ion batteries. *J. Am. Chem. Soc.* **136**, 5039–5046 (2014).

27.   Zheng, J., Lochala, J. A., Kwok, A., Deng, Z. D. & Xiao, J. Research Progress towards Understanding the Unique Interfaces between Concentrated Electrolytes and Electrodes for Energy Storage Applications. *Adv. Sci.* **4**, 1–19 (2017).

28.   Qian, J. *et al.* High rate and stable cycling of lithium metal anode. *Nat. Commun.* **6**, (2015).

29.   KUWATA, H., SONOKI, H., MATSUI, M., MATSUDA, Y. & IMANISHI, N. Surface Layer and Morphology of Lithium Metal Electrodes. *Electrochemistry* **84**, 854–860 (2016).

30.   Lee, Y. *et al.* Fluorine-incorporated interface enhances cycling stability of lithium metal batteries with Ni-rich NCM cathodes. *Nano Energy* **67**, 104309 (2020).

31.   Zhang, X. Q., Cheng, X. B., Chen, X., Yan, C. & Zhang, Q. Fluoroethylene Carbonate Additives to Render Uniform Li Deposits in Lithium Metal Batteries. *Adv. Funct. Mater.* **27**, 1–8 (2017).

32. Guo, J., Wen, Z., Wu, M., Jin, J. & Liu, Y. Vinylene carbonate-LiNO3: A hybrid additive in carbonic ester electrolytes for SEI modification on Li metal anode. *Electrochem. commun.* **51**, 59–63 (2015).

33. Sano, H., Sakaebe, H. & Matsumoto, H. Observation of electrodeposited lithium by optical microscope in room temperature ionic liquid-based electrolyte. *J. Power Sources* **196**, 6663–6669 (2011).

34. Yan, C. *et al.* Lithium Nitrate Solvation Chemistry in Carbonate Electrolyte Sustains High-Voltage Lithium Metal Batteries. *Angew. Chemie - Int. Ed.* **57**, 14055–14059 (2018).

35. Zhang, X. Q. *et al.* Regulating Anions in the Solvation Sheath of Lithium Ions for Stable Lithium Metal Batteries. *ACS Energy Lett.* **4**, 411–416 (2019).

36. Aurbach, D. *et al.* On the Surface Chemical Aspects of Very High Energy Density, Rechargeable Li–Sulfur Batteries. *J. Electrochem. Soc.* **156**, A694 (2009).

37. Xiong, S., Xie, K., Diao, Y. & Hong, X. Properties of surface film on lithium anode with LiNO 3 as lithium salt in electrolyte solution for lithium-sulfur batteries. *Electrochim. Acta* **83**, 78–86 (2012).

38. Zhang, X. Q. *et al.* Highly Stable Lithium Metal Batteries Enabled by Regulating the Solvation of Lithium Ions in Nonaqueous Electrolytes. *Angew. Chemie - Int. Ed.* **57**, 5301–5305 (2018).

39. Liu, Y. *et al.* Solubility-mediated sustained release enabling nitrate additive in carbonate electrolytes for stable lithium metal anode. *Nat. Commun.* **9**, 1–10 (2018).

40. Wang, J. Z. *et al.* Sulfur-graphene composite for rechargeable lithium batteries. *J. Power Sources* **196**, 7030–7034 (2011).

41. Adams, B. D. *et al.* Long term stability of Li-S batteries using high concentration lithium nitrate electrolytes. *Nano Energy* **40**, 607–617 (2017).

42. Zhang, X. *et al.* A Sustainable Solid Electrolyte Interphase for High-Energy-Density Lithium Metal Batteries Under Practical Conditions. *Angew. Chemie* **132**, 3278–3283 (2020).

43. Ding, N. *et al.* Building better lithium-sulfur batteries: From LiNO2 to solid oxide catalyst. *Sci. Rep.* **6**, 1–10 (2016).

44. Liang, X. *et al.* Improved cycling performances of lithium sulfur batteries with LiNO 3-modified electrolyte. *J. Power Sources* **196**, 9839–9843 (2011).

45. Rodriguez, R. *et al.* Effect of the Electrolyte on the Cycling Efficiency of Lithium-Limited Cells and their Morphology Studied Through in Situ Optical Imaging. *ACS Appl. Energy Mater.* **1**, 5830–5835 (2018).

46. Lian, F. *et al.* Preparation of LiBOB via rheological phase method and its application to mitigate voltage fade of Li1.16[Mn0.75Ni0.25]0.84O2 cathode. *RSC Adv.* **5**, 86763–86770 (2015).

47.   Wu, Q. *et al.* Effects of lithium difluoro(oxalate)borate on the performance of Li-rich composite cathode in Li-ion battery. *Electrochem. commun.* **24**, 78–81 (2012).

48.   Liu, J., Chen, Z., Busking, S. & Amine, K. Lithium difluoro(oxalato)borate as a functional additive for lithium-ion batteries. *Electrochem. commun.* **9**, 475–479 (2007).

49.   Lee, S. J. *et al.* A bi-functional lithium difluoro(oxalato)borate additive for lithium cobalt oxide/lithium nickel manganese cobalt oxide cathodes and silicon/graphite anodes in lithium-ion batteries at elevated temperatures. *Electrochim. Acta* **137**, 1–8 (2014).

50.   Han, J. G. *et al.* Interfacial Architectures Derived by Lithium Difluoro(bisoxalato) Phosphate for Lithium-Rich Cathodes with Superior Cycling Stability and Rate Capability. *ChemElectroChem* **4**, 56–65 (2017).

51.   Liao, B. *et al.* Designing Low Impedance Interface Films Simultaneously on Anode and Cathode for High Energy Batteries. *Adv. Energy Mater.* **8**, (2018).